JACS
JOURNAL OF THE AMERICAN CHEMICAL SOCIETY

Open Access
This article is licensed under CC-BY-NC-ND 4.0

pubs.acs.org/JACS
Article

Discovery of Macrocyclic Peptide Binders, Covalent Modifiers, and Degraders of a Structured RNA by mRNA Display

Xiyuan Yao, Kanokpol Aphicho, Shubhashree Pani, Anuchit Rupanya, Tong Lan, and Bryan C. Dickinson*

Cite This: https://doi.org/10.1021/jacs.5c05540
Read Online

ACCESS | Metrics & More | Article Recommendations | Supporting Information

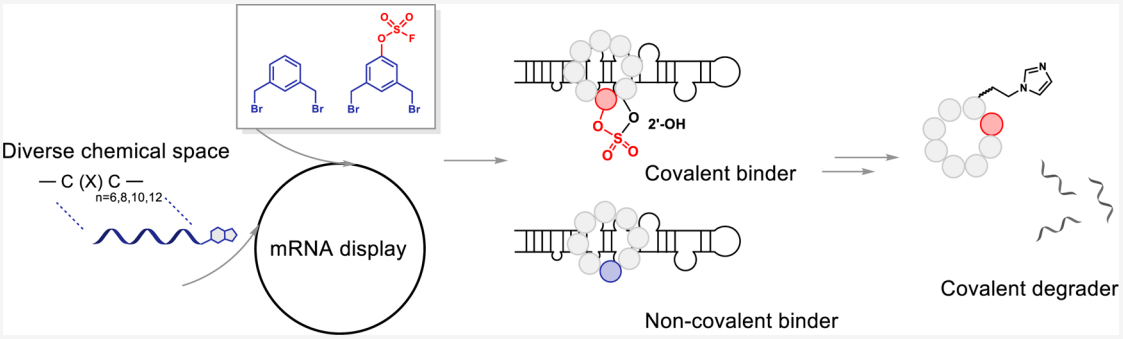

ABSTRACT: RNA targeting represents a compelling strategy for addressing challenging therapeutic targets that are otherwise intractable through traditional protein targeting. Revolutionary approaches in RNA-focused small molecule libraries have successfully identified RNA-binding ligands but generally remain limited in diversity and impeded by a dearth of structural insight into RNA and RNA complexes. Cyclic peptides are potential structural mimics of evolutionary RNA-protein interacting motifs and can be massively diversified and selected via genetically encoded libraries, offering a complementary approach. This study introduces genetically encoded thioether cyclic peptide libraries constructed through mRNA display using a dibromoxylene linker and its fluorosulfonyl derivative that can covalently engage RNA nucleophiles. Using an optimized mRNA display workflow for RNA binders, we discovered high affinity, covalent and noncovalent binders for *SNCA* 5′ UTR IRE, the upstream iron-responsive element that post-transcriptionally regulates the expression of α-synuclein, an intrinsically disordered protein implicated in Parkinsonism and related neurodegenerative diseases. Notably, a stringent selection strategy employing "base-paired" target analog counterselection enhanced specificity by deenriching nonspecific electrostatic interactions mediated by polycationic residues. Further engineering hit peptides with an imidazole tag yielded selective RNA degraders in which covalent degraders showed noticeably improved potency from noncovalent counterparts. This work provides a prototype framework for evolution-driven, high-throughput, RNA-targeted drug discovery using cyclic peptides.

Downloaded via 70.235.130.126 on September 19, 2025 at 16:51:40 (UTC).
See https://pubs.acs.org/sharingguidelines for options on how to legitimately share published articles.

INTRODUCTION

Targeting gene expression at the RNA level offers a promising approach to manipulate hard-to-target parts of the proteome, expanding the druggable space of the human genome.[1−4] Established programmable RNA-targeting strategies, including antisense oligonucleotides and guide RNA-dependent RNA regulatory systems, have demonstrated that targeting RNA can alter gene expression in cellular and animal models, often resulting in therapeutically desired phenotypes.[5−9] Small molecules targeting specific RNA structures are an alternative approach to target RNA with fewer delivery challenges, as illustrated by the first FDA-approved splicing modifier, Risdiplam, for the treatment of Spinal Muscular Atrophy (SMA).[10] However, despite these and other successes, selective small molecule discovery for RNA targets is substantially more challenging than targeting the proteome, due to RNA conformational heterogeneity, nonspecific charge interactions stemming from the highly anionic nature of RNA, and limited throughput for large-scale screening of RNA binders.[11,12]

Current state-of-the-art approaches for identifying *de novo* RNA binding small molecules have led to success in identifying drug leads for targeting important RNA functions such as translational regulation,[13,14] splicing,[15,16] miRNA maturation,[17] aberrant gain-of-function by RNA repeats.[18−20] These

Received: April 1, 2025
Revised: August 20, 2025
Accepted: August 22, 2025

ACS Publications
© XXXX The Authors. Published by American Chemical Society

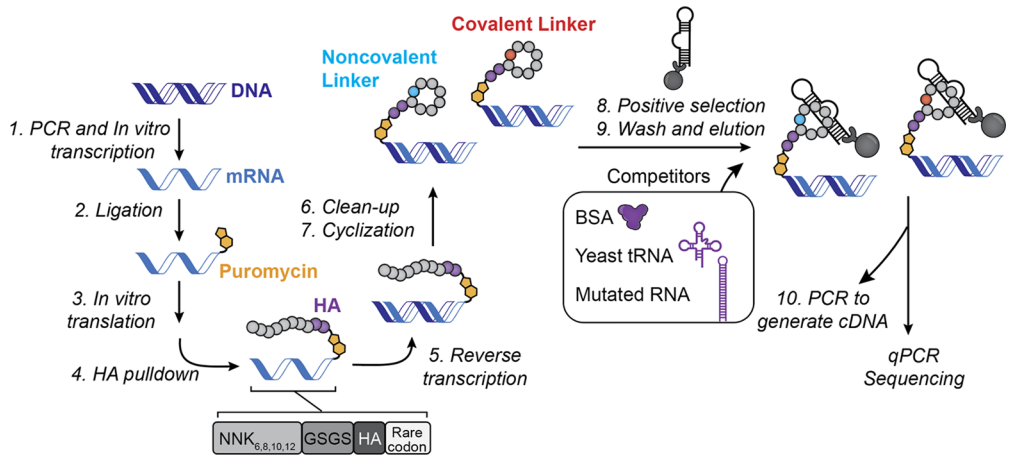

Figure 1. mRNA display for the discovery of RNA targeting cyclic peptides. Randomized DNA libraries are transcribed into mRNA and subsequently ligated to a puromycin oligonucleotide tag. Then peptides are displayed on mRNA during *in vitro* translation step. After on-bead HA pull-down, mRNAs undergo reverse transcription to generate complementary DNA (cDNA) strands. The resulting linear peptides can then be cyclized using either noncovalent or covalent linkers. Finally, the cyclic peptide libraries are subjected to positive selection against immobilized target RNA in the presence of competitors. The selected cDNAs are ultimately eluted for downstream validations and subsequent rounds of selection.

approaches often involve rational RNA-focused library design with privileged motifs coupled with covalent-assisting high-throughput screening platforms such as photo-cross-linking-based Chem-CLIP[21,22] and 2′-OH acylation-based SHAPE[23] in *in vitro* or cell-based assays.[17] However, because of the limited insight into the structural diversity of RNA and RNA-Ligand complexes, the overall chemical space derived from this knowledge is thought to be underexplored.[11]

Genetically encoded display-based screens have become popular for building larger chemical libraries to identify binders, exploiting barcoded genotype-phenotype linkage to simplify, increase throughput workflow, and enable evolution-inspired selection for complex properties.[24−26] Recent advances in constructing genetically encoded libraries have led to the discovery of potent small molecules with high selectivity for structured RNA targets using DNA-encoded chemical libraries (DECL), such as r(*CUG*)^{exp19}, primary microRNA-27a,[27] and *Escherichia coli* FMN Riboswitch.[28] The genetically encoded library of cyclic peptides offers a potentially powerful alternative strategy,[25] allowing massive sampling of the protein−surface-like conformation that potentially mirrors natural RNA-protein interaction surfaces.[28] mRNA display has been successfully exploited to discover potent macrocyclic peptide inhibitors for a wide range of therapeutically relevant protein targets.[26,29,30] The emergence of covalent targeting has inspired the development of mRNA display macrocyclic peptide containing covalent warheads as a strategy to augment potency and specificity against an even broader array of challenging targets, buoyed by success in the development of covalent inhibitors for targeting "undruggable" protein targets such as KRAS.[31,32] The fact that structured RNAs also contain reactive hot spots amenable to covalent modification by warheads brought in proximity by employing alkylating agents (ex. Chlorambucil,[18] alkyl halides,[33] epoxide[34]), diazirines,[20] activated sulfonyl groups,[35] acyl imidazoles[36] and acyl chlorides[37] presents a premise for the covalent RNA drug-target engagement.

Despite these successes, applying mRNA display for the selection of cyclic peptide libraries against structurally dynamic RNA targets is challenging. Unlike conventional medicinal chemistry strategies for designing bioactive protein inhibitors, RNA-binding molecules tend to exhibit distinct physicochemical properties, including increased polarity, larger surface areas, and more hydrogen bonding interactions.[1,38] This raises the question of whether similar structural preferences exist in peptide-RNA interactions. More importantly, another consideration in genetically encoded libraries is the inherent bias introduced by degenerate codons. Certain residues, such as arginine, serine, and leucine, are often overrepresented compared to others. Since RNA molecules possess negatively charged phosphate groups, peptides enriched with cationic residues may exhibit strong electrostatic interactions, potentially leading to nonspecific interactions during selection. Encouraged by the genetically encoded discovery of linear peptide for selective targeting RNA G-quadruplex[39] and other studies,[40−43] we aim to develop a general cyclic peptide mRNA display platform for targeting common and diverse RNA structure elements including internal loops, bulges, helices, and hairpins by carefully optimizing the library design and employing counterselection protocols for contributing to the groundwork for the discovery of RNA-targeting molecules.

In this study, we engineered an mRNA display platform for selecting RNA-binding macrocyclic peptides against the iron responsive element (IRE) region of an mRNA encoding the intrinsically disordered protein alpha-synuclein (*SNCA* 5′ UTR IRE), a structured, translation-mediating RNA linked to Parkinson's and related diseases.[44] First, we explored a strategy to install a covalent warhead on mRNA-displayed cyclic peptides via a trireactive cyclization linker in addition to the previously established dibromoxylene linker. Next, we developed a prototype based on human immunodeficiency virus (HIV) transactivation response element RNA (TAR) and its well-established interacting peptides, allowing us to build, test, and optimize the RNA-targeting cyclic peptide mRNA display pipeline. Upon the success of the model system, we moved on to our main campaign of selecting cyclic peptides against *SNCA* 5′ UTR IRE. We constructed two 10^{12} macrocyclic peptide libraries of varying peptide lengths, either with or without an aryl fluorosulfonate-based covalent warhead. We tracked the selections over the course of 10

https://doi.org/10.1021/jacs.5c05540
J. Am. Chem. Soc. XXXX, XXX, XXX−XXX

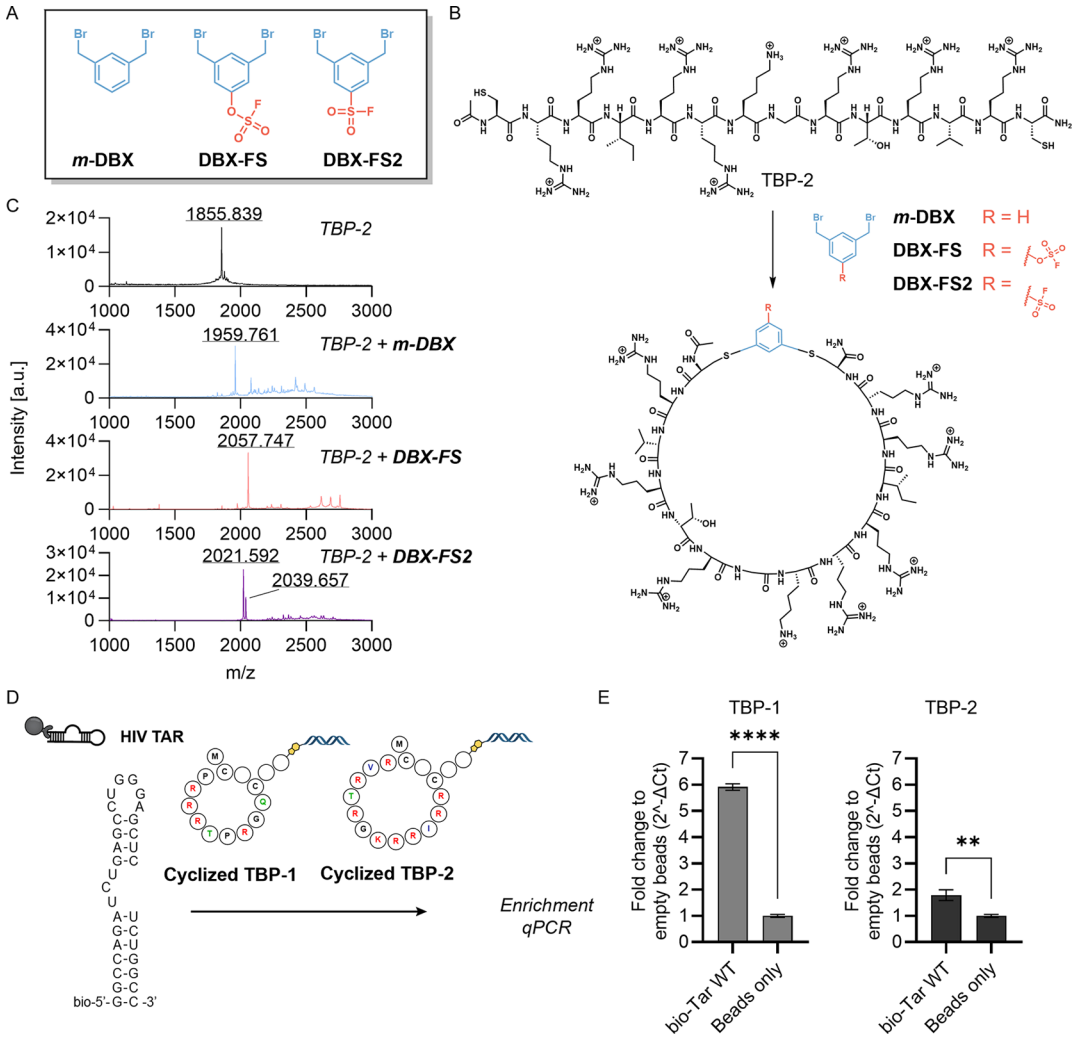

Figure 2. Linker design and cyclization validations. (A) Structures of ***m*-DBX** and covalent warhead functionalized derivatives, **DBX-FS** and **DBX-FS2**. (B) Cyclization strategy for dicysteine containing peptide. (C) MALDI-TOF characterization of cyclized TBP-2 using three different linkers (20 mM Tris HCl, pH 7.8, 200 μM TCEP, 30% acetonitrile, 1 h incubation). A minor peak observed for peptide cyclization with **DBX-FS2** (2021.592) indicates a loss of fluorine. (D) Structures of ***m*-DBX** cyclized TAR binding peptides. (E) Quantitative PCR analysis of recovered cDNA after pull-down. Experiments were performed in triplicate (n = 3); **, p = 0.0028, ****, p < 0.0001.

rounds by quantitative PCR (qPCR) and high-throughput sequencing with increasing counterselection pressure via a competition with a base-paired *SNCA* 5′ UTR IRE analog to discourage nonselective RNA binding modes. This revealed cyclic peptide sequences that putatively bind the target RNA. A secondary screen on selected hits identified covalent and noncovalent cyclic peptide binders that selectively bind the *SNCA* 5′ UTR IRE over the tested off-target RNAs with 0.6 to 17 μM affinity. Finally, we installed an imidazole pegylated tag[45] for proximity-dependent RNA degradation on the peptide binders, resulting in macrocyclic peptides that induce selective RNA degradation *in vitro*. This work established an RNA-targeting macrocyclic peptide discovery workflow and highlights the potential of cyclic peptides in advancing RNA-targeted peptide drug development.

RESULTS AND DISCUSSION

mRNA Display Workflow for Identifying Cyclic Peptides Binders to Immobilized RNA. Previously, we established a thioether-linked cyclic peptide library, which led to the discovery of potent covalent inhibitors of TEV protease.[46] In this study, we aimed to apply an analogous pipeline involving library generation via designer linker mediated cyclization using *m*-dibromoxylene (***m*-DBX**) or its derivative with a preinstalled RNA-reactive covalent warhead to identify RNA-binding peptides and developed a stringent selection strategy to enrich selective binders (Figure 1). The general architecture of the library consisted of the peptide coding region flanked by conserved sequences, including an upstream T7 promoter region for *in vitro* transcription followed by a downstream GSGS linker and an HA tag for affinity-based purification to ensure uniform, complete translation, as well as a rare codon region and binding sites for the puromycin tag via Y-ligation[47] (Figure 1). We optimized a stepwise workflow for library construction and selection: 1. PCR amplification and *in vitro* transcription of randomized DNA library; 2. RNA ligation with puromycin conjugated DNA oligonucleotide; 3. *in vitro* translation of the mRNA display cassettes and puromycin-mediated ligation of the nascent peptide chain; 4. HA pull-down of full-length puromycin-linked mRNA-peptide fusions; 5. reverse transcription resulting in duplex cDNA displayed peptides (to

https://doi.org/10.1021/jacs.5c05540
J. Am. Chem. Soc. XXXX, XXX, XXX−XXX

minimize binding interactions between the RNA sequences displaying the peptides and the target RNA[47,48]); 6. oligo-dT cleanup to polish display quality; and 7. ***m*-DBX**-mediated cyclization of full-length displayed peptides followed by oligo-dT cleanup. Next, selection and regeneration of enriched peptides (steps 8−10) are performed: 8. incubation of the displayed cyclic peptide library with immobilized RNA target with the competitors; 9. washing off unbound peptides and elution of the retained target RNA binding peptides; 10. PCR amplification of enriched cDNA library, which is subject to PCR and *in vitro* transcription to generate mRNA transcripts for the next round of selection. qPCR is performed on eluted cDNAs to assess the recovery rate as part of the in-process quality control. The amplified cDNA library is subjected to high-throughput sequencing for library characterization, allowing elucidation of the selection outcome against the target RNA of interest, *SNCA* 5′ UTR IRE. We will describe the development and optimization of this mRNA display workflow in the next sections.

DBX and Its Reactive Analogs Enable Synthesis of Noncovalent and Covalent RNA-Targeting Cyclic Peptides. Prior work identified bis-electrophiles reagents as biocompatible cross-linkers in the construction of genetically encoded cyclic dicysteine-flanked peptide libraries, including phage display and mRNA display.[49,50] In this study, we built upon previously developed ***m*-DBX**[51] and developed its derivatives installed with an RNA-targeting moiety (Figure 2A), with the goal of improving potency and selectivity. Dibromoxylene fluorosulfonate **DBX-FS** (Compound **2**) and a dibromoxylene sulfonyl fluoride **DBX-FS2** (Compound **3**), which harbor an activated fluorosulfonyl species that undergo Sulfur(VI) Fluoride Exchange (SuFEx) chemistry[52] and have been recently shown to react with 2′-OH of RNA with varying stability under physiological conditions,[35,53] were synthesized as lead RNA-targeting covalent linkers in our evaluation.

Following facile synthesis (Methods), we evaluated the cyclization utility of ***m*-DBX** and two fluorosulfonyl-containing linkers with two model peptides: somatostatin, a naturally occurring 14-aa peptide with terminal-most cysteines, and TAR-binding peptide 2 (TBP-2), a prototype linear peptide derived from previously reported HIV TAR RNA-binding peptide[54] (Figures S1−S3 and Figure 2). MALDI-TOF mass spectrometry revealed generalizability and a good agreement between somatostatin and TBP-2 cyclization (Figures S1−S3 and Figure 2C). We observed that cyclization mediated by ***m*-DBX** and **DBX-FS** proceeded with minimal side reaction within 5 min, while prolonged incubation of up to 2 h did not affect the structural integrity. The cyclization mediated by **DBX-FS2**, however, was susceptible to rapid side reactions as evidenced by the loss of F. We hypothesized that the sulfonyl fluoride warhead in the cyclized product further reacts intramolecularly with other nucleophilic residues, such as the primary amine of lysine, resulting in the observed side product. The uncontrollable reactivity of **DBX-FS2** versus the highly selective reactivity of **DBX-FS** that enabled clean and precise cyclization were consistent with the much higher reactivity of sulfonyl fluorides over fluorosulfonate, reported previously.[55] The chemical lability of sulfonyl fluoride **DBX-FS2** rendered it unsuitable for generating covalent cyclic peptide libraries that must remain intact before selection. Therefore, we proceeded with ***m*-DBX** and the fluorosulfonate **DBX-FS** as the noncovalent and covalent cyclization linkers, respectively, for generating cyclic peptide libraries in our later large-scale selection campaign against *SNCA* IRE.

Development and Optimization of RNA-Binding Cyclic-Peptide mRNA Display Workflow. We aimed to develop and optimize a streamlined *in vitro* translation and cyclization of mRNA-displayed peptides using HIV TAR[56] as a model system (Figure 2D). For simplicity, we limited cyclization to a single linker, ***m*-DBX** using previously reported HIV TAR binding peptides.[54,57] We designed TBP-1 and TBP-2 by introducing cysteine residues at both termini and obtained DBX-cross-linked cyclic TBP-1 (**DBX-cTBP-1**) and TBP-2 (**DBX-cTBP-2**).[52,54,55] (Figure 2D). Fluorescence polarization assay confirmed the derivative peptides **DBX-cTBP-1** and **DBX-cTBP-2** retain affinity to TAR RNA, with k_D values of 0.3 ± 0.07 μM and 11 ± 9 nM respectively (Figure S4).

After successful verification of the model cyclic peptides, we next sought to display them on mRNAs, in line with our designed library construction and selection workflow (Figure 1). We subjected the mRNA transcription cassettes encoding TBP-1 and TBP-2 to ligation with the puromycin tag, *in vitro* translation, HA tag cleanup, and reverse transcription, tracking progress at each step by visualizing on a UREA-PAGE gel. Consistent with previous reports,[44] the puromycin-ligated translation products were efficiently generated, representing 40−50% relative intensity of the shifted-up bands as compared to the unconjugated mRNAs appearing at the original, expected size (Figure S5, RNA+ IVTR+). Subsequent HA pull-down showed efficient recovery of the fully translated and ligated products of TBP-1, but not TBP-2, transcripts (Figure S5, RNA+ IVTR+ HA Clean-up+). As expected, the cDNA-mRNA hybrid duplex formation via reverse transcription showed the same trend, with reduced recovery of the TBP-2 peptide−oligonucleotide fusion (Figure S5, RNA+ IVTR+ HA Clean-up+ RT+,). We hypothesized that the loss of TBP-2 was due to nonspecific interactions between peptide and the anti-HA beads, likely mediated by its multiple cationic residues that hinder HA-specific pull-down and the recovery of mRNA-TBP-2 peptide fusion. Next, we evaluated the DBX-mediated on-bead versus in-solution cyclization during the post-RT Oligo dT cleanup step (Figure S6B). We found that the eluted cDNA from in-solution cyclization was recovered at an ∼300-fold higher amount than from on-bead cyclization. Together, this established an efficient workflow for cDNA-displayed DBX-cyclized model TAR binding peptides.

Model Selection Evaluation and Counterselection Strategy. We next sought to evaluate the performance of both TBP-1 and TBP-2 peptides in the model selection against immobilized TAR RNA. We first optimized the folding and immobilization of 5′-biotinylated TAR RNA on streptavidin-coated beads. Optimization of the immobilization time and wash conditions revealed that 30 min incubation at room temperature is sufficient to retain most RNA, and 2−3 washes (25 mM Tris, pH 7.5, 10 mM $MgCl_2$, 1 mg/mL BSA) can preserve immobilized RNA on the beads, with no further RNA elution from additional washes Figure S6C). Next, cDNA-displayed cyclic peptides derived from TBP-1 and TBP-2 were incubated with immobilized HIV TAR on beads in the presence of equimolar amounts of nonspecific competitors BSA and tRNA (1h at room temperature). We then eluted the cDNA-displayed peptides from beads by heat denaturation. We assessed cDNA recovery by qPCR analysis of the cDNA eluted from the bound fraction. Critically, we observed

https://doi.org/10.1021/jacs.5c05540
J. Am. Chem. Soc. XXXX, XXX, XXX−XXX

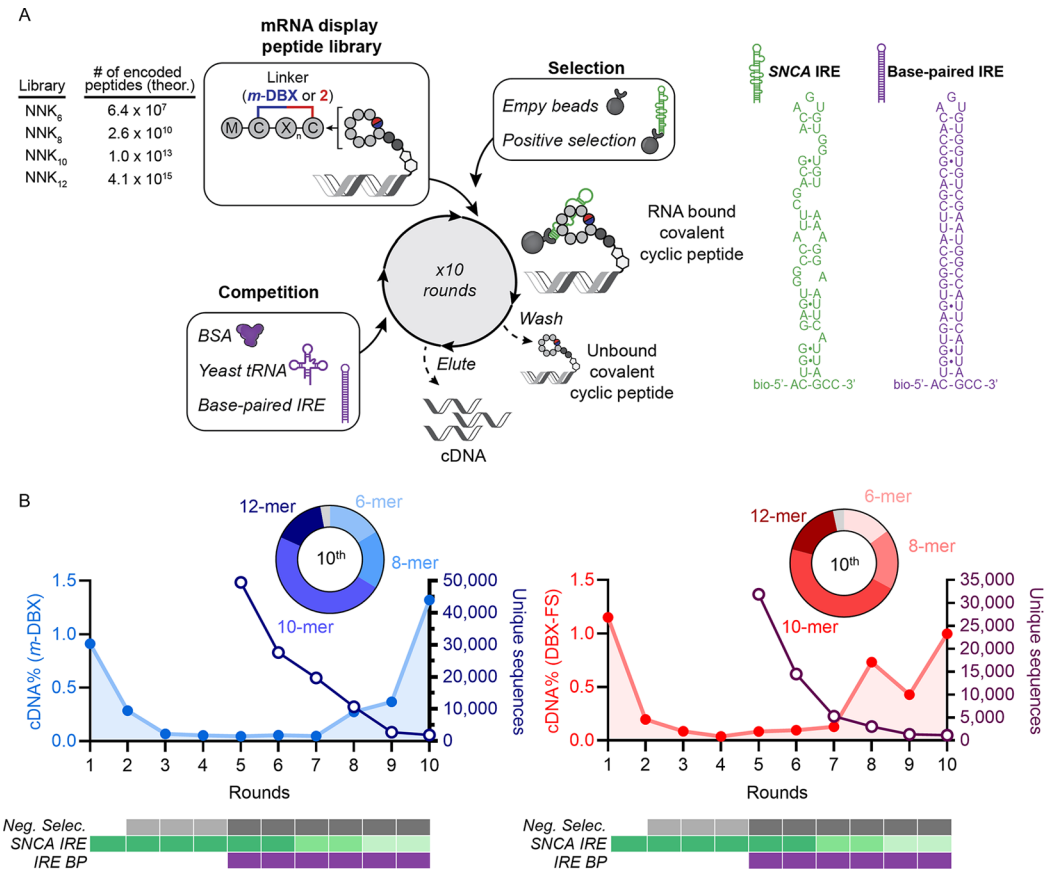

Figure 3. mRNA encoded cyclic peptide library design and selection against structured 5′ UTR IRE of *SNCA* mRNA. (A) mRNA encoded cyclic peptide library consists of 6, 8, 10, 12-mer dicysteine peptides cyclized with ***m*-DBX** or **DBX-FS**. Selections were performed against 5′-biotin labeled *SNCA* IRE in the presence of competitors, including a full base-paired RNA mutant, bovine serum albumin, yeast tRNA. (B) Selection progress monitored by quantitative PCR and high throughput sequencing. cDNA% (left axis) refers to recovery of complementary DNA from mRNA encoded library after affinity pull-down. Total number of unique sequences (right axis) was determined by sequencing analysis after removing redundant sequences. Donut plots represent the loop lengths distribution after round 10 for peptide sequences containing two cysteine residues. In ***m*-DBX** library (left), 16.4% 6-mer, 17.4% 8-mer, 48.0% 10-mer, 15.4% 12-mer; In **DBX-FS** library (right), 14.8% 6-mer, 18.1% 8-mer, 46.3% 10-mer, 17.5% 12-mer. Selections conditions are presented in the bar graph and details in Supporting Information (Table S3).

biotinylated TAR RNA-dependent enrichment for both TBP-1 and TBP-2, with a larger fold change and cDNA recovery for TBP-1 (Figure 2E, Figure S7), consistent with an earlier observation of their disparate recovery in the HA pull-down step.

To assess the competition strategy and further demonstrate that the enrichment is target RNA dependent, we performed the same experiment using cDNA-displayed, ***m*-DBX**-cyclized TBP-1 in the presence of varying excess amounts of free, nonbiotinylated HIV TAR to compete off the peptide and immobilized TAR binding interactions. Indeed, we observed a target-dependent decrease in cDNA recovery (Figure S8), suggesting that the addition of excess competitor RNAs during selection can deenrich undesirable binding interactions.

Given the successes with the RNA target-dependent recovery of the cognate peptides of a model RNA in the presence and absence of on-target competitors (Figure S8), we next turned to large-scale *de novo* cyclic peptide mRNA display. Our development of the trireactive linker, **DBX-FS**, enables covalent targeting as a potency- and selectivity-enhancing approach. We therefore hypothesized that base-paired RNA counterselection could be used to identify RNA binders with minimal or no nonspecific cationic interactions.

***De Novo* Identification of Covalent and Noncovalent Binders to *SNCA* 5′ UTR IRE via Large-Scale mRNA Display.** To showcase our successfully developed linkers and mRNA display workflow for enriching model RNA-binding peptides, we initiated a large-scale mRNA display campaign targeting an evolutionarily conserved, structured iron-responsive element (IRE) of the *SNCA* mRNA that interacts with the iron-regulatory protein (IRP). The *SNCA* IRE is located in the 5′ untranslated region (UTR) of *SNCA* mRNA, and regulates this gene's translation through an iron-dependent pathway.[58] The inhibition of the *SNCA* IRE-IRP interaction has been identified as a potential therapeutic strategy to alter translation and potentially improve *SNCA*-driven neuropatholgies. Since that the secondary structures of this IRE have been elucidated,[13] and previous studies have reported several distinct chemotypes that selectively interact with the A-bulge[13,14] within the *SNCA* IRE, we considered this RNA structure to be a ligandable target to test the efficacy of our workflow.

We designed two peptide libraries, each containing randomized codons, Cys(NNK)$_x$Cys (x = 6, 8, 10, 12), cyclized with either ***m*-DBX** or **DBX-FS**, generating libraries of up to 10^{15} theoretical variants (12-mer) (Figure 3A). 600 ng of ligated mRNA, composed of equal amounts (150 ng) of each

https://doi.org/10.1021/jacs.5c05540
J. Am. Chem. Soc. XXXX, XXX, XXX−XXX

A

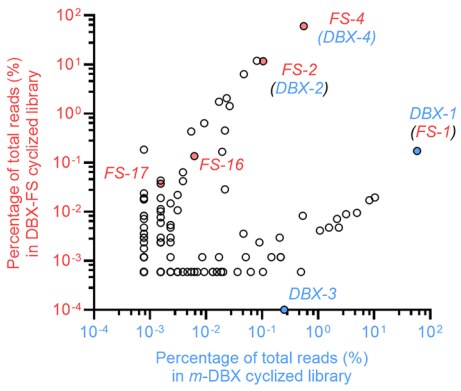

B

Name	Peptide sequence	%Reads	K_D (μM) IRE WT	K_D (μM) IRE BP	K_D (μM) TAR WT
DBX-1	MCPPTTTRWQPHC	58.4%	17.4 ± 0.3	> 100	> 100
FS-1		0.2%	5.1 ± 1.6	> 100	6.4 ± 0.01
DBX-2	MCSTTYDFRRTTRFC	0.1%	1.7 ± 0.6	> 100	3.3 ± 0.6
FS-2		11.7%	1.3 ± 0.1	9.0 ± 3.9	10.6 ± 3.6
DBX-3	MCRYKTTSMIC	0.3%	0.6 ± 0.4	> 25	2.5 ± 1.2
FS-3		NA	1.9 ± 0.2	2.9 ± 0.2	2.0 ± 0.7
DBX-4	MCSTTNMLPNLSC	0.6%	–	–	–
FS-4		60.5%	6.5 ± 2.3	–	–

C

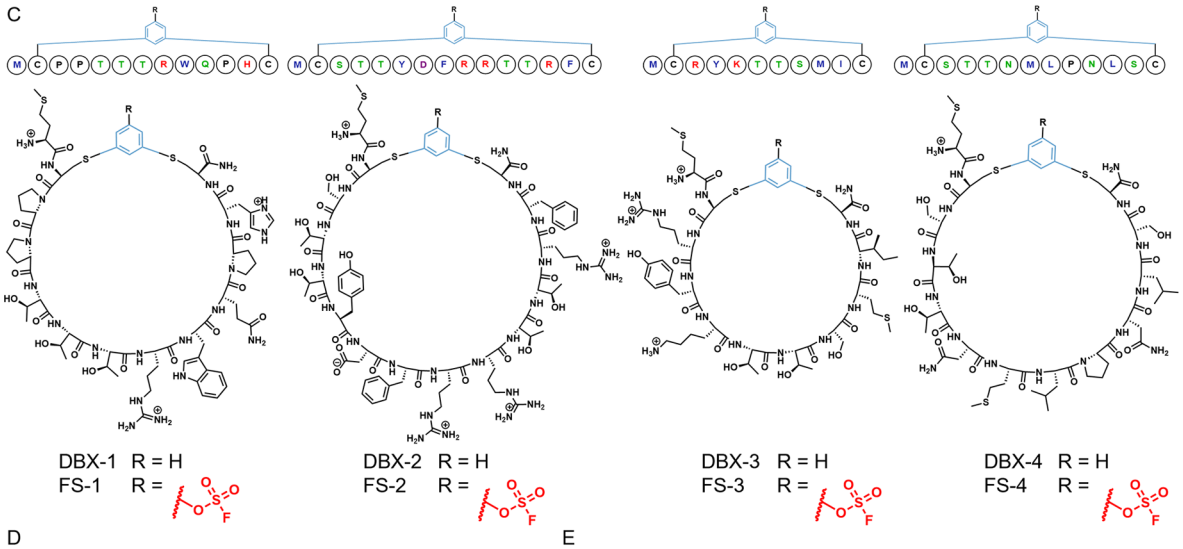

D

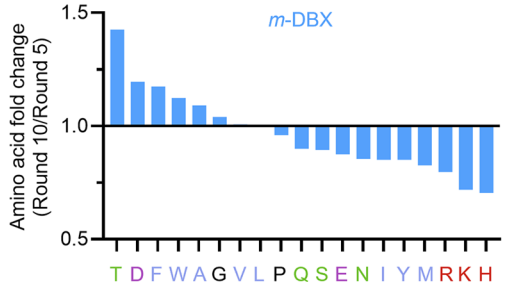

E

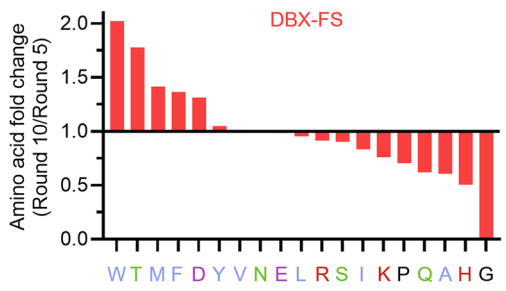

Figure 4. Selection results uncovered *SNCA* IRE binding cyclic peptides. (A) A two-dimensional plot shows enriched sequences after last round of selections for both libraries. (B) Cyclic peptide hits binding dissociation constants (K_D) measured on a 5′-FITC *SNCA* IRE (IRE WT), its base-paired mutant (IRE BP) and HIV TAR (TAR WT). Binding studies (n = 2) were performed in 20 mM HEPES, pH 7.2, 1 mM $MgCl_2$. "–" denotes that a binding curve could not be fitted due to fluctuating fluorescence signals (Figure S18). (C) Structures of cyclic peptide hits. (D, E) Fold change of 20 amino acids (exclude cysteine) for *SNCA* IRE from round 10 by normalizing to round 5. Data is normalized to translation bias for NNK degenerate codon. Amino acids are color coded according to side chains. Positively charged are highlighted in red, negatively charged in magenta, polar uncharged in green, and hydrophobic in purple.

sublibrary, was subjected to *in vitro* translation. Based on an estimated translation efficiency of 40%, the resulting peptide library was calculated to contain 2.3−2.6 × 10^{12} actual variants. This library is expected to fully cover the theoretical diversity of both $(NNK)_6$ and $(NNK)_8$ libraries and partially for the $(NNK)_{10}$ and $(NNK)_{12}$ libraries. We synthesized the *SNCA* IRE RNA with a 5′-biotin for immobilization (Figure 3A) and commenced selection.

The first round of selection was conducted using *SNCA* IRE immobilized on beads, incubated for 20 h, in the presence of BSA and yeast tRNA as competitors (Table S3). qPCR analysis showed a recovery of about 1% of each library after this round, indicating some potential enrichment that can be continued with increased selection pressure. From the second round onward, we introduced a negative selection step wherein libraries were incubated with empty beads (i.e., no immobilized target RNA) before initiating the main selection, thereby removing sequences that nonspecifically bind to the beads. Supernatants were collected and subjected to positive selection against the immobilized *SNCA* IRE. Again, we recovered 0.3−0.2% RNA from each library, indicating that stronger selection pressure decreased total enrichment. From

https://doi.org/10.1021/jacs.5c05540
J. Am. Chem. Soc. XXXX, XXX, XXX−XXX

the third round onward, we reduced the incubation time to 1 h at room temperature. Downstream qPCR analysis showed a continued decrease in recovery until the third round, indicating effective depletion of nonbinders (Figure 3B, Figure S9). The cDNA recovery stabilized between rounds three and four, where we introduced a 5-fold excess of a "base-paired" *SNCA* IRE competitor. It has been demonstrated that peptide binders are capable of distinguishing subtle differences in atomic positions in the RNA helix structure, and the addition of competitor RNA with a mutation at specific positions can direct the selection campaign for desired discrimination for RNA binding interactions or orientations in phage display campaign of linear peptide.[59] We envisioned employing a base-paired variant of the target RNA, a designed homologue with all putative secondary structures mutated to be complementary, as a competitive binding partner during the selection process would suppress nonspecific contacts while largely retaining as many diverse chemotypes as possible to engage distinct loops, bulges, and other distinct structural elements in the target RNAs of interest. We therefore spiked in 5-fold excess of the competitor base-paired, nonbiotinylated RNA (*SNCA* IRE BP; Table S3) to outcompete undesired binding interactions to the immobilized RNA target.

In the following selection rounds, we maintained a steady amount of the *SNCA* IRE BP competitor and further increased the selection stringency in round seven by reducing the amount of immobilized on-target *SNCA* IRE RNA. By round eight, we began to observe an increase in cDNA recovery for both libraries, with an overall increasing trend over the final three rounds. After round ten, qPCR validation of cDNA libraries generated with and without corresponding linker confirmed that the majority of enriched sequences are linker dependent (Figure S10) and the cDNA libraries enriched using 5′-bio-*SNCA* IRE or 5′-bio-*SNCA* IRE BP confirmed that the total library is *SNCA* IRE specific. Overall, these results indicate potential enrichment of IRE-specific cyclic peptide binders. Therefore, we next sought to characterize the selection outcomes from both libraries.

Sequencing Reveals Convergent and Divergent Evolution of Target RNA-Binding Peptides. We analyzed selections by next generation sequencing (NGS) at each round to track the progress of the selection. As the last three rounds of selection showed a dramatic increase in cDNA recovery, we speculated that significant changes in library variants and diversity occurred in these rounds. Comparison of sequencing reads from the last six rounds of selection revealed that as the selection stringency increased, the number of unique peptide sequences rapidly fell, with <2000 variants in the ***m*-DBX** cyclized library and 1165 in the **DBX-FS** cyclized library (Figure 3B). Interestingly, a small subset of sequences became highly enriched, reflected by high sequencing read counts (Figure 4A). By round ten, despite the two libraries being developed from the same initial library pool, the two different cyclization methods yielded distinct sets of enriched peptide sequences (Figure 4A). For example, the most abundant sequence enriched from the **DBX-FS** cyclized library accounted for 60.5% of the total sequencing reads for that library, but only 0.6% in the ***m*-DBX** cyclized library (Figure 4B). Although several top peptide hits were largely convergent between the selection of ***m*-DBX** and the **DBX-FS** generated library, the significant portion of divergently evolved peptides points to an unexpected influence of covalence on binding modes that result in distinct sets of unique peptides identified from each of the two libraries.

Among the four different peptide lengths contained in the initial libraries, sequences containing ten amino acids between the two cysteines were the most enriched, followed by 12-mer and 8-mer (Figures S11−S12). Although the theoretical number of variants in the 10-mer (1×10^{13}) or 12-mer (4.1×10^{15}) libraries exceeds the practical coverage of an mRNA display library, we observed consistent increases in both unique sequences and total variants for 10-mer and 12-mer peptides over the last six selection rounds, and decreases for 6-mer and 8-mer peptides (Figure S12). This trend was observed in both the ***m*-DBX** and **DBX-FS** cyclized libraries, suggesting that distinct cyclic peptide sizes are preferred for *SNCA* IRE binding. Further analysis of the cysteine content confirmed that peptides containing two cysteines were the predominant species in both libraries (Figure S13). Although the NNK degenerate codon set used in library design allows for the incorporation of cysteine, sequences containing more than two cysteines were limited in selection outcomes. This suggests that cyclic peptide structures are favored over alternative structures for binding the *SNCA* IRE.

Biophysical Characterization of Cyclic Peptide Binders for *SNCA* IRE. Encouraged by the sequencing results, we proceeded with binding affinity measurements to determine the dissociation constant (K_D) of the enriched peptide variants. We first sorted all peptide sequences from the last round of each selection based on their sequencing reads. To perform clustering analysis and visualize the peptide convergence, molecular fingerprints of each cyclic peptide were computed using extended-connectivity fingerprints (ECFPs) and embedded in 2D t-distributed Stochastic Neighbor Embedding (t-SNE).[60] ECFPs is a method for representing chemical structures for the purpose of clustering and similarity searching[61] and recently applied to peptide library analysis.[62,63] Peptides from the ***m*-DBX** library with high abundance and located at distinct sequence families (Figure S14) were selected for solid phase peptide synthesis. Among them, sequences that are common between the two libraries were cyclized with either the ***m*-DBX** or the **DBX-FS** linker. After purification, we measured the binding affinities of these peptides to *SNCA* IRE using fluorescence polarization (FP). FP measures changes in molecular rotation[64] upon binding, and is widely used for studying nucleic acid-peptide[65] and nucleic acid-small molecule[66] interactions. For FP experiments, we used *SNCA* IRE with 5′-fluorescein to track binding.

The top enriched sequence (58.4%) from the ***m*-DBX** cyclized library (DBX-1), a C-10_{mer}-C peptide, exhibited a K_D of 17.4 ± 0.3 μM with the *SNCA* IRE. DBX-1 did not show binding as a linear peptide and, when tested against the base-paired IRE control RNA or HIV TAR, showed unsaturated binding, indicating only nonspecific interactions at high concentration (Figure S15). Taken together, these results confirm that the selection was successful and that the protocol could enrich selective RNA binding peptides. Of note, DBX-1 contains just a single cationic residue (R), with a higher propensity for H-donor and hydrophobic residues, in line with the observed selectivity in binding, which does not appear to be electrostatic driven, as with the TAR-binding peptides used as references.

We selected two additional sequences from the selection, DBX-2 (a C-12_{mer}-C peptide) and DBX-3 (a C-8_{mer}-C peptide), for characterization. While DBX-2 and DBX-3 had

https://doi.org/10.1021/jacs.5c05540
J. Am. Chem. Soc. XXXX, XXX, XXX−XXX

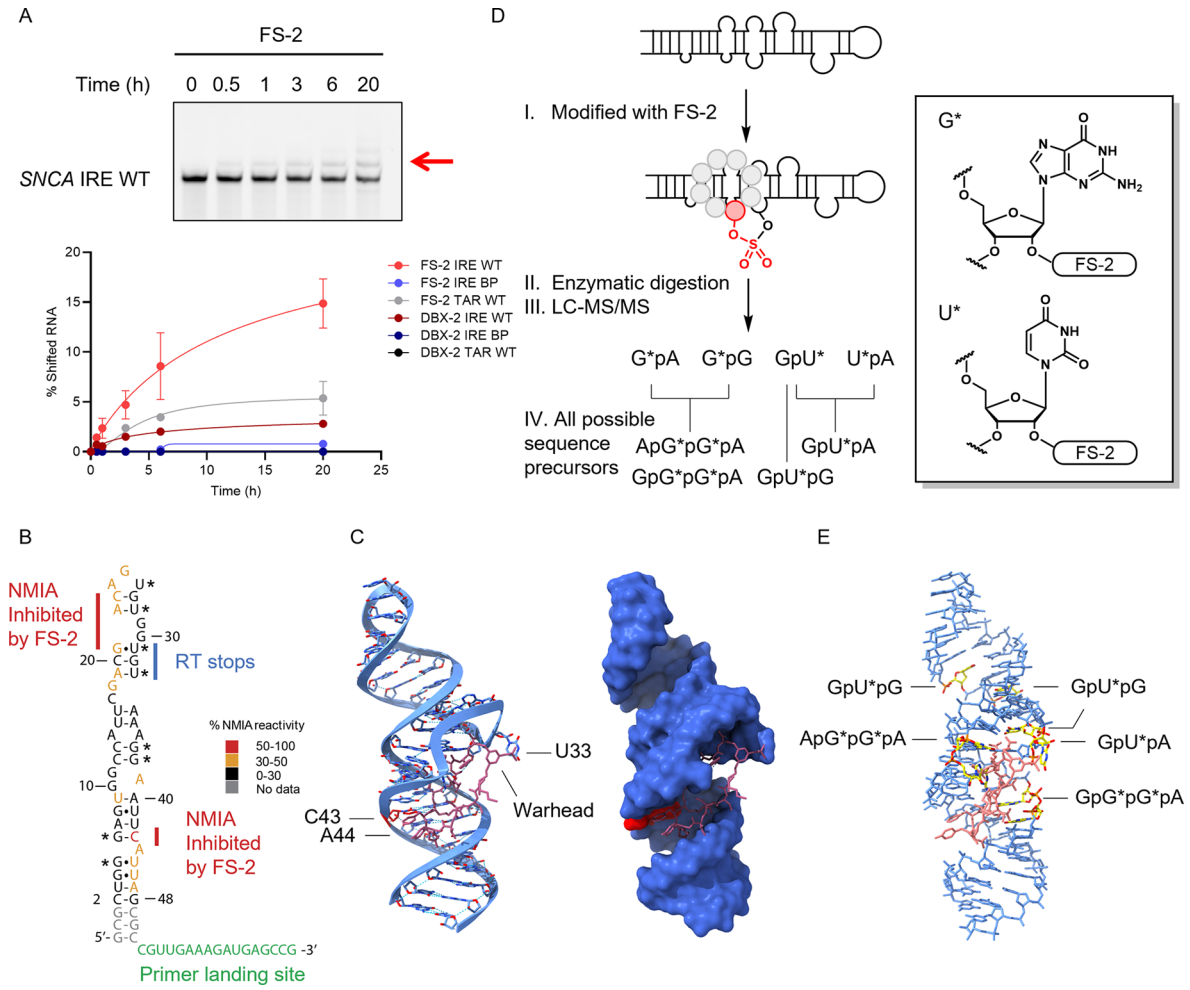

Figure 5. Covalent peptide hits showed selective gel shift with *SNCA* IRE and triggers RT-stop signals. (A) The selectivity of the covalent peptide hit FS-2 (50 μM) was assessed by denaturing PAGE using 0.5 μM *SNCA* IRE (IRE WT), a base-paired RNA control (IRE BP) and HIV TAR (TAR WT). Reactions were performed in 20 mM HEPES buffer (pH 7.5), 1 mM $MgCl_2$, and incubated at 37 °C. (B) *In vitro* SHAPE experiments using NMIA were performed to identify reactive nucleotides. RNA preincubated with FS-2 (10 μM, h) showed a strong decrease in NMIA reactivity at C43 and A24 (highlighted in red). Incubation with varying concentrations of FS-2 for 24 h resulted in prominent RT stops around U31. Asterisks denote all possible FS-2 labeling sites from LC-MS/MS experiments. (C) Predicted 3D structure of the *SNCA* IRE (primer landing site removed) and proposed docking pose of FS-2. (D) Enzymatic digestion and LC-MS/MS analysis of FS-2 labeled *SNCA* IRE. FS-2 modification was identified at GpG*, G*pA, GpU*, and U*pA dinucleotides via sulfonylation at 2′-hydroxyl group. (E) Alignment of all possible digestion tri-, tetra- nucleotide precursors revealed accessibility of the reactive warhead near the binding site.

lower percentage reads in the final selection, they also bound *SNCA* IRE, with K_D values of 1.7 ± 0.6 and 0.6 ± 0.4 μM (Figure 4B, Figure S14), respectively. Again, no saturated binding curves could be fitted for the base-paired RNA control. In contrast, a 2- or 4- fold selectivity was observed for IRE WT over HIV TAR respectively further supporting the specificity of these interactions. This confirms that in addition to the top variant in the selections, lower abundance sequences, including those of different macrocycle sizes, also selectively bind the target RNA.

Next, we shifted our attention to **DBX-FS** cyclized library hits. We synthesized the DBX-1, DBX-2 and DBX-3 peptide sequences as **DBX-FS** cyclized peptides (FS-1, FS-2 and FS-3), and again measured their binding to *SNCA* IRE. All showed binding, with K_D's of 5.1 ± 1.6, 1.3 ± 0.1, and 1.9 ± 0.2 μM, respectively (Figures S15–S17). Of note, only FS-2 was abundant in the **DBX-FS** cyclized library selection outcome, showing that the linker change did not dramatically alter binding. Finally, we selected the most enriched sequence from the **DBX-FS** cyclized library selection (60.5% of sequences), which was low abundance in the ***m*-DBX** library (0.6%). We synthesized and tested this peptide both as the **DBX-FS** cyclized peptide (FS-4) and as the *m*-DBX cyclized peptide (DBX-4). FS-4 showed *SNCA* IRE binding of 6.5 ± 2.3 μM K_D, while the DBX-4 counterpart showed unstable binding (Figure S18). Collectively, these data confirm the selections successfully enriched unique peptides with both linkers and that mRNA-display can enrich macrocycles that selectively bind target RNA, without sole reliance on charge−charge interactions. We next analyzed the sequencing data to gain insights into the RNA binding peptide features.

NGS Analysis Reveals Features for Cyclic Peptide Binders for *SNCA* IRE. Known RNA binding peptides often rely on charge−charge interactions, with cationic residues such as Lys and Arg dominating sequences. As a clear illustration of this, the TAR-binding peptides used for our initial validation each contain a majority of cationic residues. We were therefore intrigued that the enriched peptides in the *SNCA* IRE

https://doi.org/10.1021/jacs.5c05540
J. Am. Chem. Soc. XXXX, XXX, XXX−XXX

selection, which featured a strong counterselection to enforce selective binding, did not contain highly cationic sequences (Figure 4B).

To better understand the global amino acid composition that allowed target binding, we analyzed the shift in frequency amino acid composition from round five, where sequences were still quite random, through the subsequently more selective six rounds of selection, ending at round ten (Figure S19). Indeed, this analysis revealed a progressive decrease over time in polar, charged side chain containing residues such as Arg, His, and Lys. Similarly, highly translated residues, such as Ser, Gly, Ala and Pro also exhibited a general decline (Figure 4D−E, Figure S19). More importantly, aromatic π-containing residues such as Phe, Trp, and Asp, which are capable of potential nitrogenous base stacking interactions, tended to increase. Overall, incorporating competitor RNAs and stringent conditions during the selection proved to be critical for identifying selective RNA binding peptides, which resulted in peptide compositions that are not highly enriched for cationic residues usually associated with nonselective nucleic acid binding.

Covalent RNA-Binding Peptides Induce Covalent Adduct Formation. We next aimed to test whether any of the peptides cyclized with **DBX-FS** form covalent adducts with the *SNCA* IRE. We selected the 11 representative sequences from clustering analysis (Figure S14) in the **DBX-FS** cyclized library and screened them for covalent adduct formation with *SNCA* IRE using a denaturing electrophoretic gel mobility shift assay. Among the 11 sequences tested, four (FS-2, FS-4, FS-16 and FS-17) exhibited selective band shifts with *SNCA* IRE (peptide to RNA, 100:1) after a 4-h incubation at room temperature (20 mM HEPES, pH 7.5, 1 mM $MgCl_2$) (Figures S20−S21). These results suggest a potential hit rate of 36% for covalent cyclic peptide binders within this library. Furthermore, extending the incubation time to 24 h led to an increased covalent adduct formation, with up to 33% of RNA-peptide complexes with minimal shift observed with base-paired RNA. These results indicate that the fluorosulfonyl warhead yields covalent hits and generates covalent adducts more efficiently compared to previous epoxide-based probes[34] that react with a self-alkylating RNA (*cis* epoxide probe to RNA, 1300:1).

We selected FS-2 for further validation due to its high reactivity and performed a time course analysis of covalent adduct formation (Figure 5, Figures S22−S23). The RNA-peptide covalent complex is detectable within 30 min of incubation and gradually increased over 24 h. Notably, FS-2 is highly selective against *SNCA* IRE and exhibited negligible reactivity toward the base-paired IRE or HIV TAR which was not used in the selection. FS-2 exhibits dose-dependent RNA labeling with k_{inact} = 0.003611 min^{-1} and K_I = 0.000105 M (k_{inact}/K_I = 34.4 M^{-1} min^{-1}) (Figures S24−S25). Increasing the ionic strength or adding BSA had a minimal impact on RNA labeling efficiency (Figure S26). In comparison, three other DBX-FS cyclized peptide hits showed weaker binding correlated to lower reactivity, suggesting a proximity driven binding mechanism (Figure 4B, Figure S22).

Testing warhead stability showed FS-2 remains relatively stable at 25 °C pH 7.5 over 24 h (Figure S27) and during scaled-up synthesis (Figure S28). However, a slowly forming decomposition product was observed upon extended incubation (Figure S27) and became more pronounced at increased temperature and higher pH values (Figures S29−S30). These observations are consistent with previous findings on TBP-2 cyclization using DBX-FS2, suggesting that the fluorosulfonate group may undergo intramolecular reactions with nucleophilic side chain bearing residues within the cyclic peptide scaffold, leading to the formation of bicyclic structures. Moreover, although fluorosulfonate warheads are known to react with common nucleophilic residues such as Tyr/Lys/Ser/His,[67] FS-2 exhibited undetectable intermolecular reactivity with these amino acids (Figures S31−S32).

Collectively, these results demonstrate that **DBX-FS** cyclized peptide libraries combined with an mRNA display can uncover covalent binders specific to target RNA structures. And peptides with higher binding affinity exhibit increased covalent reactivity with RNA. We next aimed to study the binding modes of both noncovalent and covalent peptide hits in more detail.

Nucleotides Modified Most with SHAPE Reagents Are Inhibited Most upon Hit Peptide Binding. To investigate the structural dynamics of *SNCA* IRE, we employed Selective 2′-Hydroxyl Acylation analyzed by Primer Extension (SHAPE),[68] a method widely used to detect flexible RNA regions by covalently modifying the 2′-OH of the ribose rings with acylating probes, such as NMIA. Analysis of the terminated cDNA products from *SNCA* IRE revealed that nucleotide C43 close to the A-bulge at the bottom stem is the most NMIA-reactive nucleotide, followed by C23 near the apical loop and A22, A24 (Figures S33, S34, S35B). Notably, the highest degree of modification was observed at the bottom stem -AC- motifs, suggesting that a constrained small bulge is likely formed at the position, making them reactive to the SHAPE reagent.[69] Unstructured loops and bulges in RNA are common sites for perturbation during ligand binding. Previous studies have reported that small molecules can selectively interact with the A-bulge of *SNCA* IRE.[13,14]

We next tested how peptide binding alters SHAPE labeling on the *SNCA* IRE to uncover potential sites of interaction. Preincubating *SNCA* IRE with ***m*-DBX** peptide hits DBX-1, DBX-2 and DBX-3 for 30 min at room temperature resulted in a strong reduction in NMIA labeling for both C43 and C23 (Figures S33, S35C). This observation is consistent with **DBX-FS** cyclized peptide hits, FS-2 and FS-4 (Figures S34, S35C), suggesting that peptide binding inhibits the NMIA acylation activity, likely due to a binding event that blocks the accessibility of the 2′-OH toward NMIA or induced conformational constrain.[70] Furthermore, the model RNA used in SHAPE experiments, without a primer landing site (green), was used to predict a folded 3D structure by Boltz-1.[71,72] Docking poses generated with FS-2 suggest that the cyclic peptide is likely engaged with the bottom helix structure through multiple hydrogen bonding networks (Figure S36), leaving the apical loops flexible and less structured. These predicted H-bonds are mainly formed between the amides on the peptide backbone, with key residues such as Arg, Ser, and Thr interacting with ribonucleotide structures including nucleobases, ribose 2′−OH and phosphate groups. The docking poses suggest that the covalent warhead could be positioned close to U33 and that the entire cyclic peptide fits inside the RNA major groove. Indeed, by incubating 100 μM FS-2 and model RNA for 24 h at 37 °C, the complex can induce reverse transcription stop signals (RT stops) primarily before U31 (Figure 5B, Figure S37) in a concentration dependent manner, lending evidence to this model. Altogether, these mapping experiments lend credence to a model in which

https://doi.org/10.1021/jacs.5c05540
J. Am. Chem. Soc. XXXX, XXX, XXX−XXX

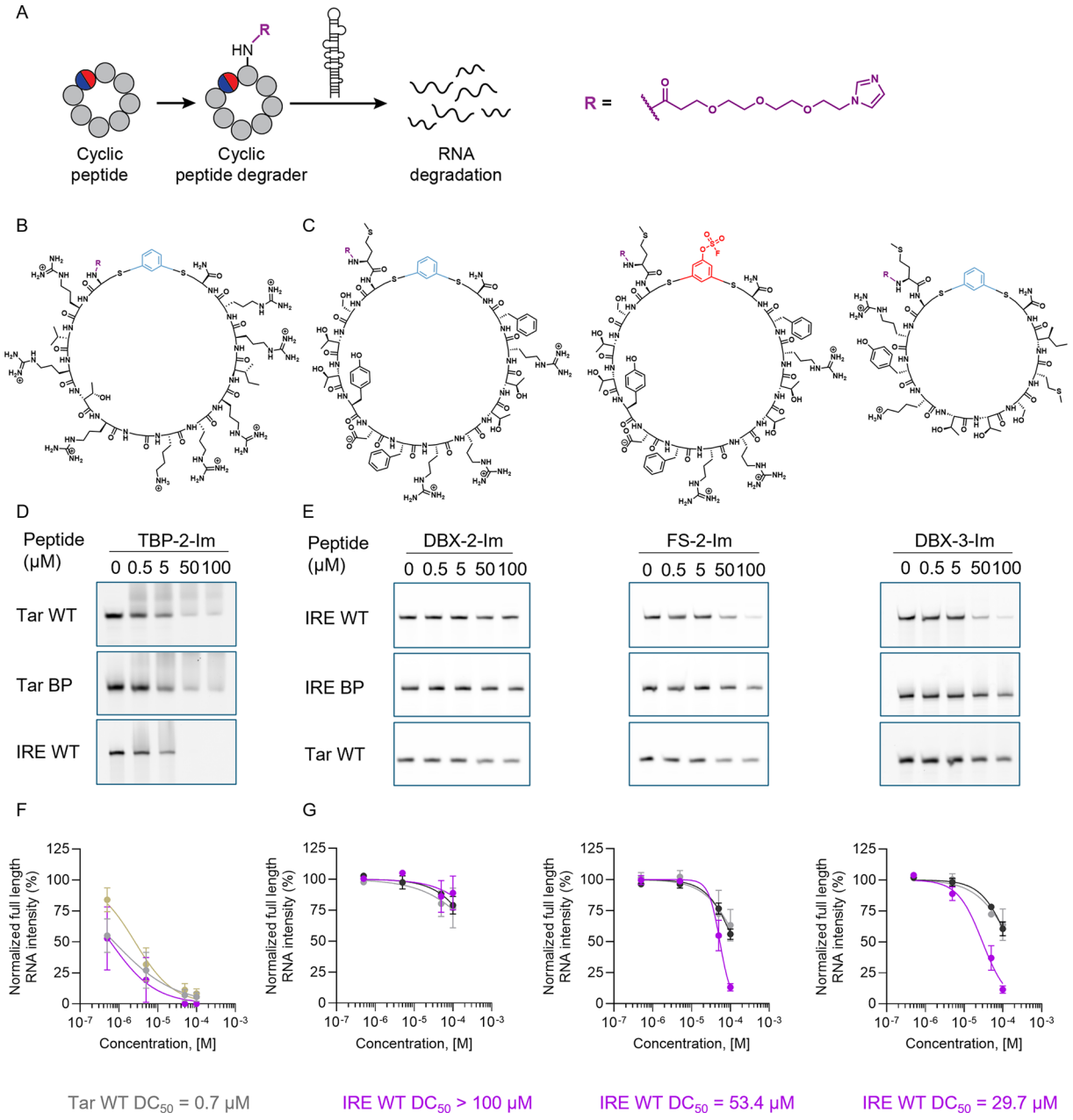

Figure 6. Selective RNA degradation by imidazole functionalized cyclic peptides. (A) Design strategy for imidazole functionalized cyclic peptides for RNA degradation. (B,C) Chemical structures of cyclic peptide degraders derived from TBP-2 and three hit cyclic peptides from selection. (D,E) Dose-dependent RNA cleavage assays analyzed by 15% denaturing PAGE. RNA (0.5 μM) was incubated with peptide degraders for 6 h at 37 °C in 20 mM HEPES buffer (pH 7.5) 1 mM $MgCl_2$ and 40 μg/mL BSA. (F,G) Quantification of full-length RNA band intensities, normalized to the no compound control. Error bars represent the standard error of the mean from two independent experiments.

the *SNCA* IRE is ligandable by cyclic peptides with a possible induced binding pocket in the bottom helix of the structure (Figure 5C).

RNA Digestion Coupled with Tandem Mass Spectrometry Reveals FS-2 Labeling Sites. To investigate the covalent bond formation between FS-2 and the target RNA, the *SNCA* IRE RNA was incubated with FS-2 at 25 °C overnight. RNA samples were subsequently purified and digested by using a nuclease cocktail. These digested samples were then separated by reversed-phase HPLC and analyzed by electrospray mass spectrometry. Identified precursor ions were further fragmented with MS/MS to identify the sequence context for adduct formation and fragmentation patterns. Four dinucleotide adducts were detected including GpG*, G*pA, ApU* and U*pG (asterisks denote FS-2 modified nucleotide) and ionization up to four charged states were observed (Figure 5D, Figures S38−S40). The formation of these cyclic peptide-nucleoside complexes could likely cause incomplete nuclease digestion due to steric hindrance, stopping the nuclease activity at dinucleotide adducts. MS/MS fragmentation patterns for all four species indicate sulfonylation of the 2′-hydroxyl group, which weakens the glycosidic bond (−O−SO_3-). Moreover, fragments generated from phosphate diester bond cleavages further confirmed the identity of the labeled nucleoside (Figures S41−S44).

https://doi.org/10.1021/jacs.5c05540
J. Am. Chem. Soc. XXXX, XXX, XXX−XXX

The fact that only guanosine and uridine were modified among the four dinucleotides provides the sequence information for uncovering probable labeling sites on RNA. Assuming the modified nucleotide site is shared among the two dinucleotide adducts observed, we found that the labeled uridine flanking with A/G is only present as GpU*pA within the *SNCA* IRE (Figure 5B) near the observed RT stop sites. Similarly, the labeled uridine flanking with guanosine could be GpU*pG, and the labeled guanosine flanking with A/G could likely be ApGpGpA or GpGpGpA. Mapping all these possible digestion precursors on the RNA structure revealed that they are within reach of the FS-2 warhead in the docking pose (Figure 5E). Overall, these observations provide direct evidence of covalent bond formation via 2′ hydroxyl sulfonylation.

Selective RNA Degradation Achieved by Imidazole Functionalized Cyclic Peptide Binders. Finally, we tested whether the peptide binders could be used for proximity-induced RNA degradation. Previously, proximity-induced RNA degradation has been achieved by small molecules by recruiting endogenous nucleases,[73] transition-metal catalyzed oxidation reaction,[20] and by small molecules functionalized with an imidazole, mimicking RNase A and catalyzing the direct cleavage of the RNA target.[45,74,75] We selected the three top peptide hits and engineered them into potential RNA degraders by installing imidazole-PEG_3 on the N-terminal side of the peptide sequence using solid phase synthesis to generate DBX-2-Im, FS-2-Im, and DBX-3-Im (Figure 6A−C). In addition, we also synthesized the nonselective TAR binding cyclic peptide TBP-2 as a putative degrader (TBP-2-Im).

We incubated TBP-2-Im with HIV TAR, the TAR BP, and the *SNCA* IRE for 6 h at 37 °C, during which time we observed a dose-dependent degradation of all three RNAs (Figure 6D, 6F, Figure S45). This is expected due to the nonspecific binding of the TBP-2 peptide and reaffirms that the TBP-2-Im is a nonspecific small molecule RNA nuclease. Next, we repeated these experiments with DBX-2-Im, FS-2-Im, and DBX-3-Im. While DBX-2-Im only showed weak nonspecific degradation (Figure S46), both FS-2-Im and DBX-3-Im (Figure 6E, 6G) showed significant *SNCA* IRE degradation with less activity on either the base-paired IRE control or the HIV TAR off-target RNA. We analyzed the sites of cleavage of FS-2-Im by RNA gel, and intriguingly, we observed major cleavage bands at C23 and C43 (Figure S47). Both nucleotides are highly reactive with NMIA in SHAPE experiments, suggesting the apical loop on *SNCA* IRE is flexible and accessible enough for imidazole-dependent RNA degradation but in a proximity-dependent manner as mediated by peptide binding. Further testing of FS-2-Im under conditions of increased ionic strength and excess BSA revealed minimal impact on RNA degradation (Figure S48) and the compound exhibited stability comparable to that of FS-2 (Figures S49−S50). These data indicate that FS-2-Im and DBX-3-Im are both small molecule RNA nucleases and that tighter binding (by comparing DBX-2 and DBX-3) and more selective binding (by comparing TBP-2 and FS-2/DBX-4) are essential considerations for designing selective peptide-based RNA degraders.

CONCLUSIONS

In this study, we established a pipeline for discovering cyclic peptides targeting the *SNCA* IRE using an mRNA display, enabling sampling of trillions of peptide-RNA interactions. We took advantage of established benzyl bromide as synthesis scaffold and designed new linkers that are efficient at cyclization with high yield. Notably, we found that covalent peptides containing a fluorosulfonate warhead are compatible with the *in vitro* selection process in line with selection using phage display,[76] leading to the successful discovery of covalent *SNCA* IRE targeting peptides. Finally, we demonstrated that cyclic peptide hits identified from the mRNA display workflow can be further engineered into selective RNA degraders.

A major challenge in any selection, but even more so in mRNA-based selections for RNA binders, is nonspecific binding interactions between the negatively charged surfaces of DNA barcodes, mRNA barcodes, or phages and attached molecules or displayed peptides. In mRNA display, incorporating a reverse transcription step for the mRNA-peptide conjugates before selection has been shown to reduce nonspecific binding and increase stability.[47,77] Other approaches, such as the use of charge-neutralizing peptides, have also demonstrated reduced nonspecific interactions.[78] We implemented multiple strategies to mitigate nonspecific binding, including negative selection with empty beads, coincubation with excess equivalents of mutated target RNA, and the addition of blocking agents such as BSA and yeast tRNA over extended selection rounds. Critically, we used a very strong counterselection pressure using carefully crafted structural analogues, specifically the base-paired structure. As a result, we observed a progressively decreasing trend in the enrichment of cationic residues such as arginine, histidine, and lysine during the selections, which normally dominate the RNA binders. From a structural standpoint, we found that among the enriched dicysteine-containing peptides, 10-amino acid cycles emerged as the most prevalent population for *SNCA* IRE binding. This is intuitively reasonable; RNA binding is challenging for small molecules, and the additional contacts and flexibility associated with larger cycles yield more potent hits.

Additional studies are needed to demonstrate the functional consequences of hit peptide binding, through either biochemical or cell-based assays. Previous work has shown that small molecules targeting the *SNCA* IRE can reduce translation level by decreasing the amount of *SNCA* mRNA loaded into polysomes.[13] Whether the cyclic peptides identified in this study can elicit a similar effect remains to be determined. Future efforts could also focus on unnatural amino acid incorporation[63,79] and structural modifications.[80,81] These strategies may lead to RNA targeting peptides with improved pharmacological properties and cellular permeability.

Covalent targeting of RNA holds significant therapeutic potential, although further optimization is needed. We observed that increased RNA labeling and degradation activity were correlated with stronger binding affinity, strengthening the importance of high affinity and selective interactions for effective covalent modification. Future efforts focused on structural modification of the warhead to maximize labeling efficiency and chemical stability are logical next steps.[33] Furthermore, cyclic peptide binders discovered from *in vitro* selection and structural validations can further be used for subsequent peptide engineering using alternative covalent warheads, such as alkylating reagents[34,82] for labeling nucleobases, that may not be compatible with the selection process but offer improved reactivity and stability for labeling RNA. Such strategies could expand the toolkit for RNA targeted covalent therapeutics.

https://doi.org/10.1021/jacs.5c05540
J. Am. Chem. Soc. XXXX, XXX, XXX−XXX

Overall, this study establishes a generalizable approach for the *de novo* discovery of cyclic peptide binders for structured RNA targets. This strategy has the potential to be applied in the development of peptide-based RNA biotechnologies and, potentially, starting points for therapeutic development. More broadly, this work builds on a wealth of exciting work showcasing the potential of expanding the ligandability of the transcriptome for downstream peptide-based RNA therapeutics development.

■ ASSOCIATED CONTENT

Supporting Information

The Supporting Information is available free of charge at https://pubs.acs.org/doi/10.1021/jacs.5c05540.

Materials and methods, additional tables, figures, and schemes, and general procedures (PDF)

Original sequencing data from selections (ZIP)

■ AUTHOR INFORMATION

Corresponding Author

Bryan C. Dickinson − *Department of Chemistry, University of Chicago, Chicago, Illinois 60637, United States; Chan Zuckerberg Biohub, Chicago, Illinois 60642, United States;* orcid.org/0000-0002-9616-1911; Email: dickinson@uchicago.edu

Authors

Xiyuan Yao − *Department of Chemistry, University of Chicago, Chicago, Illinois 60637, United States;* orcid.org/0000-0002-2331-0023

Kanokpol Aphicho − *Department of Chemistry, University of Chicago, Chicago, Illinois 60637, United States;* orcid.org/0000-0002-4607-1061

Shubhashree Pani − *Department of Chemistry, University of Chicago, Chicago, Illinois 60637, United States*

Anuchit Rupanya − *Department of Chemistry, University of Chicago, Chicago, Illinois 60637, United States*

Tong Lan − *Department of Chemistry, University of Chicago, Chicago, Illinois 60637, United States;* orcid.org/0000-0003-3923-5408

Complete contact information is available at: https://pubs.acs.org/10.1021/jacs.5c05540

Notes

The authors declare no competing financial interest.

■ ACKNOWLEDGMENTS

This work was supported by The G. Harold and Leila Y. Mathers Charitable Foundation, Dr. Ralph and Marian Falk Medical Research Trust, Bank of America, Private Bank, and the National Institute of Biomedical Imaging and Bioengineering of the National Institutes of Health (EB035016). We thank Jack W. Szostak and Chuan He for sharing equipment. We acknowledge valuable discussions on sequencing analysis from Aleksandar Radakovic and Ben Colville, S. Ahmadiantehrani for editing assistance, and Tongyao Wei, Riley Sinnott, Jian Zhang, and Yanfeng Xing for technical assistance.

■ REFERENCES

(1) Childs-Disney, J. L.; Yang, X.; Gibaut, Q. M. R.; Tong, Y.; Batey, R. T.; Disney, M. D. Targeting RNA Structures with Small Molecules. *Nature Reviews Drug Discovery.* **2022**, *21*, 736−762.

(2) Falese, J. P.; Donlic, A.; Hargrove, A. E. Targeting RNA with Small Molecules: From Fundamental Principles towards the Clinic. *Chemical Society Reviews.* **2021**, *50*, 2224−2243.

(3) Warner, K. D.; Hajdin, C. E.; Weeks, K. M. Principles for Targeting RNA with Drug-like Small Molecules. *Nat. Rev. Drug Discov* **2018**, *17* (8), 547−558.

(4) Kovachka, S.; Panosetti, M.; Grimaldi, B.; Azoulay, S.; Di Giorgio, A.; Duca, M. Small Molecule Approaches to Targeting RNA. *Nature Reviews Chemistry.* **2024**, *8*, 120−135.

(5) Rauch, S.; He, E.; Srienc, M.; Zhou, H.; Zhang, Z.; Dickinson, B. C. Programmable RNA-Guided RNA Effector Proteins Built from Human Parts. *Cell* **2019**, *178* (1), 122−134.e12.

(6) Cao, Y.; Liu, H.; Lu, S. S.; Jones, K. A.; Govind, A. P.; Jeyifous, O.; Simmons, C. Q.; Tabatabaei, N.; Green, W. N.; Holder, J. L.; Tahmasebi, S.; George, A. L.; Dickinson, B. C. RNA-Based Translation Activators for Targeted Gene Upregulation. *Nat. Commun.* **2023**, *14* (1), 6827.

(7) Setten, R. L.; Rossi, J. J.; Han, S.-p. The Current State and Future Directions of RNAi-Based Therapeutics. *Nature Reviews Drug Discovery.* **2019**, *18*, 421−446.

(8) Abudayyeh, O. O.; Gootenberg, J. S.; Essletzbichler, P.; Han, S.; Joung, J.; Belanto, J. J.; Verdine, V.; Cox, D. B. T.; Kellner, M. J.; Regev, A.; Lander, E. S.; Voytas, D. F.; Ting, A. Y.; Zhang, F. RNA Targeting with CRISPR-Cas13. *Nature* **2017**, *550* (7675), 280−284.

(9) Khorkova, O.; Stahl, J.; Joji, A.; Volmar, C. H.; Wahlestedt, C. Amplifying Gene Expression with RNA-Targeted Therapeutics. *Nature Reviews Drug Discovery.* **2023**, *22*, 539−561.

(10) Ratni, H.; Ebeling, M.; Baird, J.; Bendels, S.; Bylund, J.; Chen, K. S.; Denk, N.; Feng, Z.; Green, L.; Guerard, M.; Jablonski, P.; Jacobsen, B.; Khwaja, O.; Kletzl, H.; Ko, C. P.; Kustermann, S.; Marquet, A.; Metzger, F.; Mueller, B.; Naryshkin, N. A.; Paushkin, S. V.; Pinard, E.; Poirier, A.; Reutlinger, M.; Weetall, M.; Zeller, A.; Zhao, X.; Mueller, L. Discovery of Risdiplam, a Selective Survival of Motor Neuron-2 (SMN2) Gene Splicing Modifier for the Treatment of Spinal Muscular Atrophy (SMA). *J. Med. Chem.* **2018**, *61* (15), 6501−6517.

(11) Taghavi, A.; Springer, N. A.; Zanon, P. R. A.; Li, Y.; Li, C.; Childs-Disney, J. L.; Disney, M. D. The Evolution and Application of RNA-Focused Small Molecule Libraries. *RSC Chemical Biology.* **2025**, *6*, 510−527.

(12) Rhodes, C.; Balaratnam, S.; Yazdani, K.; Seshadri, S.; Schneekloth, J. S. Targeting RNA-Protein Interactions with Small Molecules: Promise and Therapeutic Potential. *Medicinal Chemistry Research.* **2024**, *33*, 2050−2065.

(13) Zhang, P.; Park, H.-J.; Zhang, J.; Junn, E.; Andrews, R. J.; Pradeep Velagapudi, S.; Abegg, D.; Vishnu, K.; Costales, M. G.; Childs-Disney, J. L.; Adibekian, A.; Moss, W. N.; Maral Mouradian, M.; Disney, M. D.; Carver, R. J. Translation of the Intrinsically Disordered Protein α-Synuclein Is Inhibited by a Small Molecule Targeting Its Structured MRNA. *Proc. Natl. Acad. Sci. U. S. A.* **2020**, *117*, 1457−1467.

(14) Tong, Y.; Zhang, P.; Yang, X.; Liu, X.; Zhang, J.; Grudniewska, M.; Jung, I.; Abegg, D.; Liu, J.; Childs-Disney, J. L.; Gibaut, Q. M. R.; Haniff, H. S.; Adibekian, A.; Mouradian, M. M.; Disney, M. D. Decreasing the Intrinsically Disordered Protein A-Synuclein Levels by Targeting Its Structured MRNA with a Ribonuclease-Targeting Chimera. *Proc. Natl. Acad. Sci. U. S. A.* **2024**, *121* (2), No. e2306682120.

(15) Fedorova, O.; Jagdmann, G. E.; Adams, R. L.; Yuan, L.; Van Zandt, M. C.; Pyle, A. M. Small Molecules That Target Group II Introns Are Potent Antifungal Agents. *Nat. Chem. Biol.* **2018**, *14* (12), 1073−1078.

(16) Silvestri, I.; Manigrasso, J.; Andreani, A.; Brindani, N.; Mas, C.; Reiser, J. B.; Vidossich, P.; Martino, G.; McCarthy, A. A.; De Vivo, M.; Marcia, M. Targeting the Conserved Active Site of Splicing Machines with Specific and Selective Small Molecule Modulators. *Nat. Commun.* **2024**, *15* (1), 4980.

(17) Suresh, B. M.; Li, W.; Zhang, P.; Wang, K. W.; Yildirim, I.; Parker, C. G.; Disney, M. D. A General Fragment-Based Approach to

Identify and Optimize Bioactive Ligands Targeting RNA. *Proc. Natl. Acad. Sci. U. S. A.* **2020**, *117*, 33197−33203.
(18) Rzuczek, S. G.; Colgan, L. A.; Nakai, Y.; Cameron, M. D.; Furling, D.; Yasuda, R.; Disney, M. D. Precise Small-Molecule Recognition of a Toxic CUG RNA Repeat Expansion. *Nat. Chem. Biol.* **2017**, *13* (2), 188−193.
(19) Gibaut, Q. M. R.; Akahori, Y.; Bush, J. A.; Taghavi, A.; Tanaka, T.; Aikawa, H.; Ryan, L. S.; Paegel, B. M.; Disney, M. D. Study of an RNA-Focused DNA-Encoded Library Informs Design of a Degrader of a r(CUG) Repeat Expansion. *J. Am. Chem. Soc.* **2022**, *144* (48), 21972−21979.
(20) Gibaut, Q. M. R.; Bush, J. A.; Tong, Y.; Baisden, J. T.; Taghavi, A.; Olafson, H.; Yao, X.; Childs-Disney, J. L.; Wang, E. T.; Disney, M. D. Transcriptome-Wide Studies of RNA-Targeted Small Molecules Provide a Simple and Selective r(CUG)Exp Degrader in Myotonic Dystrophy. *ACS Cent Sci.* **2023**, *9* (7), 1342−1353.
(21) Velagapudi, S. P.; Li, Y.; Disney, M. D. A Cross-Linking Approach to Map Small Molecule-RNA Binding Sites in Cells. *Bioorg. Med. Chem. Lett.* **2019**, *29* (12), 1532−1536.
(22) Tong, Y.; Gibaut, Q. M. R.; Rouse, W.; Childs-Disney, J. L.; Suresh, B. M.; Abegg, D.; Choudhary, S.; Akahori, Y.; Adibekian, A.; Moss, W. N.; Disney, M. D. Transcriptome-Wide Mapping of Small-Molecule RNA-Binding Sites in Cells Informs an Isoform-Specific Degrader of QSOX1MRNA. *J. Am. Chem. Soc.* **2022**, *144* (26), 11620−11625.
(23) Zeller, M. J.; et al. SHAPE-Enabled Fragment-Based Ligand Discovery for RNA Contributed New Reagents/Analytic Tools; M. *Proc. Natl. Acad. Sci. U. S. A.* **2022**, *119* (20), No. e2122660119.
(24) Yang, X.; Childs-Disney, J. L.; Paegel, M.; Disney, M. D. DNA-Encoded Libraries and Their Application to RNA. *Isr. J. Chem.* **2023**, *63* (10−11), No. e202300073.
(25) Colas, K.; Bindl, D.; Suga, H. Selection of Nucleotide-Encoded Mass Libraries of Macrocyclic Peptides for Inaccessible Drug Targets. *Chem. Rev.* **2024**, *124*, 12213−12241.
(26) Huang, Y.; Wiedmann, M. M.; Suga, H. RNA Display Methods for the Discovery of Bioactive Macrocycles. *Chem. Rev.* **2019**, *119*, 10360−10391.
(27) Benhamou, R. I.; Suresh, B. M.; Tong, Y.; Cochrane, W. G.; Cavett, V.; Vezina-Dawod, S.; Abegg, D.; Childs-Disney, J. L.; Adibekian, A.; Paegel, B. M.; Disney, M. D. DNA-Encoded Library versus RNA-Encoded Library Selection Enables Design of an Oncogenic Noncoding RNA Inhibitor. *Proc. Natl. Acad. Sci. U. S. A.* **2022**, *119*, No. e2114971119.
(28) Chen, Q.; Li, Y.; Lin, C.; Chen, L.; Luo, H.; Xia, S.; Liu, C.; Cheng, X.; Liu, C.; Li, J.; Dou, D. Expanding the DNA-Encoded Library Toolbox: Identifying Small Molecules Targeting RNA. *Nucleic Acids Res.* **2022**, *50* (12), No. E67.
(29) Iskandar, S. E.; Bowers, A. A. MRNA Display Reaches for the Clinic with New PCSK9 Inhibitor. *ACS Med. Chem. Lett.* **2022**, *13* (9), 1379−1383.
(30) Josephson, K.; Ricardo, A.; Szostak, J. W. MRNA Display: From Basic Principles to Macrocycle Drug Discovery. *Drug Discovery Today.* **2014**, *19*, 388−399.
(31) Tamura, T.; Kawano, M.; Hamachi, I. Targeted Covalent Modification Strategies for Drugging the Undruggable Targets. *Chem. Rev.* **2025**, *125*, 1191−1253.
(32) Vinogradov, A. A.; Yin, Y.; Suga, H. Macrocyclic Peptides as Drug Candidates: Recent Progress and Remaining Challenges. *J. Am. Chem. Soc.* **2019**, *141*, 4167−4181.
(33) Bereiter, R.; Flemmich, L.; Nykiel, K.; Heel, S.; Geley, S.; Hanisch, M.; Eichler, C.; Breuker, K.; Lusser, A.; Micura, R. Engineering Covalent Small Molecule−RNA Complexes in Living Cells. *Nat. Chem. Biol.* **2025**, *21*, 843.
(34) McDonald, R. I.; Guilinger, J. P.; Mukherji, S.; Curtis, E. A.; Lee, W. I.; Liu, D. R. Electrophilic Activity-Based RNA Probes Reveal a Self-Alkylating RNA for RNA Labeling. *Nat. Chem. Biol.* **2014**, *10* (12), 1049−1054.
(35) Chatterjee, S.; Shioi, R.; Kool, E. T. Sulfonylation of RNA 2′-OH Groups. *ACS Cent Sci.* **2023**, *9* (3), 531−539.
(36) Fang, L.; Velema, W. A.; Lee, Y.; Xiao, L.; Mohsen, M. G.; Kietrys, A. M.; Kool, E. T. Pervasive Transcriptome Interactions of Protein-Targeted Drugs. *Nat. Chem.* **2023**, *15* (10), 1374−1383.
(37) Pani, S.; Qiu, T.; Kentala, K.; Azizi, S. A.; Dickinson, B. C. Bioorthogonal Masked Acylating Agents for Proximity-Dependent RNA Labelling. *Nat. Chem.* **2024**, *16* (5), 717−726.
(38) Morgan, B. S.; Forte, J. E.; Culver, R. N.; Zhang, Y.; Hargrove, A. E. Discovery of Key Physicochemical, Structural, and Spatial Properties of RNA-Targeted Bioactive Ligands. *Angew. Chem.* **2017**, *129* (43), 13683−13687.
(39) Mou, X.; Kwok, C. K. Peptides Selected by G4-MRNA Display-Seq Enable RNA G-Quadruplex Recognition and Gene Regulation. *J. Am. Chem. Soc.* **2023**, *145* (34), 18693−18697.
(40) Nishikawa, S.; Watanabe, H.; Terasaka, N.; Katoh, T.; Fujishima, K. De Novo Single-Stranded RNA-Binding Peptides Discovered by Codon-Restricted MRNA Display. *Biomacromolecules* **2024**, *25* (1), 355−365.
(41) Giacobelli, V. G.; Fujishima, K.; Lepšík, M.; Tretyachenko, V.; Kadavá, T.; Makarov, M.; Bednárová, L.; Novák, P.; Hlouchová, K. In Vitro Evolution Reveals Noncationic Protein-RNA Interaction Mediated by Metal Ions. *Mol. Biol. Evol.* **2022**, *39* (3), No. msac032.
(42) Kumachi, S.; Husimi, Y.; Nemoto, N. An RNA Binding Peptide Consisting of Four Types of Amino Acid by in Vitro Selection Using CDNA Display. *ACS Omega* **2016**, *1* (1), 52−57.
(43) Iannuzzelli, J. A.; Bonn, R.; Hong, A. S.; Anitha, A. S.; Jenkins, J. L.; Wedekind, J. E.; Fasan, R. Cyclic Peptides Targeting the SARS-CoV-2 Programmed Ribosomal Frameshifting RNA from a Multiplexed Phage Display Library. *Chem. Sci.* **2024**, *15* (46), 19520−19533.
(44) Rogers, J. T.; Mikkilineni, S.; Cantuti-Castelvetri, I.; Smith, D. H.; Huang, X.; Bandyopadhyay, S.; Cahill, C. M.; Maccecchini, M. L.; Lahiri, D. K.; Greig, N. H. The Alpha-Synuclein 5′untranslated Region Targeted Translation Blockers: Anti-Alpha Synuclein Efficacy of Cardiac Glycosides and Posiphen. *J. Neural Transm (Vienna)* **2011**, *118* (3), 493−507.
(45) Mikutis, S.; Rebelo, M.; Yankova, E.; Gu, M.; Tang, C.; Coelho, A. R.; Yang, M.; Hazemi, M. E.; Pires De Miranda, M.; Eleftheriou, M.; Robertson, M.; Vassiliou, G. S.; Adams, D. J.; Simas, J. P.; Corzana, F.; Schneekloth, J. S.; Tzelepis, K.; Bernardes, G. J. L. Proximity-Induced Nucleic Acid Degrader (PINAD) Approach to Targeted RNA Degradation Using Small Molecules. *ACS Cent Sci.* **2023**, *9* (5), 892−904.
(46) Lan, T.; Peng, C.; Yao, X.; Chan, R. S. T.; Wei, T.; Rupanya, A.; Radakovic, A.; Wang, S.; Chen, S.; Lovell, S.; Snyder, S. A.; Bogyo, M.; Dickinson, B. C. Discovery of Thioether-Cyclized Macrocyclic Covalent Inhibitors by MRNA Display. *J. Am. Chem. Soc.* **2024**, *146* (34), 24053−24060.
(47) Reyes, S. G.; Kuruma, Y.; Fujimi, M.; Yamazaki, M.; Eto, S.; Nishikawa, S.; Tamaki, S.; Kobayashi, A.; Mizuuchi, R.; Rothschild, L.; Ditzler, M.; Fujishima, K. PURE MRNA Display and CDNA Display Provide Rapid Detection of Core Epitope Motif via High-Throughput Sequencing. *Biotechnol. Bioeng.* **2021**, *118* (4), 1702.
(48) Wilson, D. S.; Keefe, A. D.; Szostak, J. W. The Use of MRNA Display to Select High-Affinity Protein-Binding Peptides. *Proc. Natl. Acad. Sci. U. S. A.* **2001**, *98*, 3750−3755.
(49) Guillen Schlippe, Y. V.; Hartman, M. C. T.; Josephson, K.; Szostak, J. W. In Vitro Selection of Highly Modified Cyclic Peptides That Act as Tight Binding Inhibitors. *J. Am. Chem. Soc.* **2012**, *134* (25), 10469−10477.
(50) Chen, S.; Lovell, S.; Lee, S.; Fellner, M.; Mace, P. D.; Bogyo, M. Identification of Highly Selective Covalent Inhibitors by Phage Display. *Nat. Biotechnol.* **2021**, *39* (4), 490−498.
(51) Villequey, C.; Zurmühl, S. S.; Cramer, C. N.; Bhusan, B.; Andersen, B.; Ren, Q.; Liu, H.; Qu, X.; Yang, Y.; Pan, J.; Chen, Q.; Münzel, M. An Efficient MRNA Display Protocol Yields Potent Bicyclic Peptide Inhibitors for FGFR3c: Outperforming Linear and Monocyclic Formats in Affinity and Stability. *Chem. Sci.* **2024**, *15* (16), 6122−6129.

https://doi.org/10.1021/jacs.5c05540
J. Am. Chem. Soc. XXXX, XXX, XXX−XXX

(52) Homer, J. A.; Xu, L.; Kayambu, N.; Zheng, Q.; Choi, E. J.; Kim, B. M.; Sharpless, K. B.; Zuilhof, H.; Dong, J.; Moses, J. E. Sulfur Fluoride Exchange. *Nature Reviews Methods Primers* **2023**, *3* (1), 58.
(53) Sun, W.; Wang, N.; Liu, H.; Yu, B.; Jin, L.; Ren, X.; Shen, Y.; Wang, L. Genetically Encoded Chemical Crosslinking of RNA in Vivo. *Nat. Chem.* **2023**, *15* (1), 21−32.
(54) Davidson, A.; Leeper, T. C.; Athanassiou, Z.; Patora-Komisarska, K.; Karn, J.; Robinson, J. A.; Varani, G. Simultaneous Recognition of HIV-1 TAR RNA Bulge and Loop Sequences by Cyclic Peptide Mimics of Tat Protein. *Proc. Natl. Acad. Sci. U. S. A.* **2009**, *106* (29), 11931−11936.
(55) Zheng, Q.; Woehl, J. L.; Kitamura, S.; Santos-Martins, D.; Smedley, C. J.; Li, G.; Forli, S.; Moses, J. E.; Wolan, D. W.; Sharpless, K. B. SuFEx-Enabled, Agnostic Discovery of Covalent Inhibitors of Human Neutrophil Elastase. *Proc. Natl. Acad. Sci. U. S. A.* **2019**, *116* (38), 18808−18814.
(56) Ott, M.; Geyer, M.; Zhou, Q. The Control of HIV Transcription: Keeping RNA Polymerase II on Track. *Cell Host and Microbe.* **2011**, *10*, 426−435.
(57) Chavali, S. S.; Mali, S. M.; Bonn, R.; Anitha, A. S.; Bennett, R. P.; Smith, H. C.; Fasan, R.; Wedekind, J. E. Cyclic Peptides with a Distinct Arginine-Fork Motif Recognize the HIV Trans-Activation Response RNA in Vitro and in Cells. *J. Biol. Chem.* **2021**, *297* (6), No. 101390.
(58) Zhou, Z. D.; Tan, E. K. Iron Regulatory Protein (IRP)-Iron Responsive Element (IRE) Signaling Pathway in Human Neurodegenerative Diseases. *Molecular Neurodegeneration.* **2017**, *12*, 75.
(59) Frugier, M.; Schimmel, P. Subtle Atomic Group Discrimination in the RNA Minor Groove. *Proc. Natl. Acad. Sci. U. S. A.* **1997**, *94*, 11291−11294.
(60) Van Der Maaten, L.; Hinton, G. Visualizing Data Using T-SNE. *Journal of machine learning research* **2008**, 2579−2605.
(61) Rogers, D.; Hahn, M. Extended-Connectivity Fingerprints. *J. Chem. Inf Model* **2010**, *50* (5), 742−754.
(62) Mohapatra, S.; Hartrampf, N.; Poskus, M.; Loas, A.; Gómez-Bombarelli, R.; Pentelute, B. L. Deep Learning for Prediction and Optimization of Fast-Flow Peptide Synthesis. *ACS Cent Sci.* **2020**, *6* (12), 2277−2286.
(63) Vinogradov, A. A.; Zhang, Y.; Hamada, K.; Kobayashi, S.; Ogata, K.; Sengoku, T.; Goto, Y.; Suga, H. A Compact Reprogrammed Genetic Code for De Novo Discovery of Proteolytically Stable Thiopeptides. *J. Am. Chem. Soc.* **2024**, *146* (12), 8058−8070.
(64) Haniff, H. S.; Knerr, L.; Chen, J. L.; Disney, M. D.; Lightfoot, H. L. Target-Directed Approaches for Screening Small Molecules against RNA Targets. *SLAS Discovery.* **2020**, *25*, 869−894.
(65) Blakeley, B. D.; McNaughton, B. R. Synthetic RNA Recognition Motifs That Selectively Recognize HIV-1 Trans-Activation Response Element Hairpin RNA. *ACS Chem. Biol.* **2014**, *9* (6), 1320−1329.
(66) Wang, J.; Schultz, P. G.; Johnson, K. A. Mechanistic Studies of a Small-Molecule Modulator of SMN2 Splicing. *Proc. Natl. Acad. Sci. U. S. A.* **2018**, *115* (20), E4604−E4612.
(67) Jones, L. H. Emerging Utility of Fluorosulfate Chemical Probes. *ACS Med. Chem. Lett.* **2018**, *9* (7), 584−586.
(68) Wilkinson, K. A.; Merino, E. J.; Weeks, K. M. Selective 2′-Hydroxyl Acylation Analyzed by Primer Extension (SHAPE): Quantitative RNA Structure Analysis at Single Nucleotide Resolution. *Nat. Protoc* **2006**, *1* (3), 1610−1616.
(69) Xiao, L.; Fang, L.; Kool, E. T. Acylation Probing of "Generic" RNA Libraries Reveals Critical Influence of Loop Constraints on Reactivity. *Cell Chem. Biol.* **2022**, *29* (8), 1341−1352.e8.
(70) Merino, E. J.; Wilkinson, K. A.; Coughlan, J. L.; Weeks, K. M. RNA Structure Analysis at Single Nucleotide Resolution by Selective 2′-Hydroxyl Acylation and Primer Extension (SHAPE). *J. Am. Chem. Soc.* **2005**, *127* (12), 4223−4231.
(71) Wohlwend, J.; Corso, G.; Passaro, S.; Reveiz, M.; Leidal, K.; Swiderski, W.; Portnoi, T.; Chinn, I.; Silterra, J.; Jaakkola, T.; Barzilay, R. Boltz-1: Democratizing Biomolecular Interaction Modeling. *BioRxiv* (Biophysics). November 20, 2024. DOI: 10.1101/2024.11.19.624167 (Posted 2025-05-06).
(72) Abramson, J.; Adler, J.; Dunger, J.; Evans, R.; Green, T.; Pritzel, A.; Ronneberger, O.; Willmore, L.; Ballard, A. J.; Bambrick, J.; Bodenstein, S. W.; Evans, D. A.; Hung, C. C.; O'Neill, M.; Reiman, D.; Tunyasuvunakool, K.; Wu, Z.; Žemgulytė, A.; Arvaniti, E.; Beattie, C.; Bertolli, O.; Bridgland, A.; Cherepanov, A.; Congreve, M.; Cowen-Rivers, A. I.; Cowie, A.; Figurnov, M.; Fuchs, F. B.; Gladman, H.; Jain, R.; Khan, Y. A.; Low, C. M. R.; Perlin, K.; Potapenko, A.; Savy, P.; Singh, S.; Stecula, A.; Thillaisundaram, A.; Tong, C.; Yakneen, S.; Zhong, E. D.; Zielinski, M.; Žídek, A.; Bapst, V.; Kohli, P.; Jaderberg, M.; Hassabis, D.; Jumper, J. M. Accurate Structure Prediction of Biomolecular Interactions with AlphaFold 3. *Nature* **2024**, *630* (8016), 493−500.
(73) Tong, Y.; Lee, Y.; Liu, X.; Childs-Disney, J. L.; Suresh, B. M.; Benhamou, R. I.; Yang, C.; Li, W.; Costales, M. G.; Haniff, H. S.; Sievers, S.; Abegg, D.; Wegner, T.; Paulisch, T. O.; Lekah, E.; Grefe, M.; Crynen, G.; Van Meter, M.; Wang, T.; Gibaut, Q. M. R.; Cleveland, J. L.; Adibekian, A.; Glorius, F.; Waldmann, H.; Disney, M. D. Programming Inactive RNA-Binding Small Molecules into Bioactive Degraders. *Nature* **2023**, *618* (7963), 169−179.
(74) Martin, C.; Bonnet, M.; Patino, N.; Azoulay, S.; Di Giorgio, A.; Duca, M. Design, Synthesis, and Evaluation of Neomycin-Imidazole Conjugates for RNA Cleavage. *ChemPlusChem.* **2022**, *87* (11), No. e202200250.
(75) Nguyen, L.; Luu, L. M.; Peng, S.; Serrano, J. F.; Chan, H. Y. E.; Zimmerman, S. C. Rationally Designed Small Molecules That Target Both the DNA and RNA Causing Myotonic Dystrophy Type 1. *J. Am. Chem. Soc.* **2015**, *137* (44), 14180−14189.
(76) Wang, S.; Faucher, F. F.; Bertolini, M.; Kim, H.; Yu, B.; Cao, L.; Roeltgen, K.; Lovell, S.; Shanker, V.; Boyd, S. D.; Wang, L.; Bartenschlager, R.; Bogyo, M. Identification of Covalent Cyclic Peptide Inhibitors Targeting Protein−Protein Interactions Using Phage Display. *J. Am. Chem. Soc.* **2025**, *147*, 7461−7475.
(77) Yamaguchi, J.; Naimuddin, M.; Biyani, M.; Sasaki, T.; Machida, M.; Kubo, T.; Funatsu, T.; Husimi, Y.; Nemoto, N. CDNA Display: A Novel Screening Method for Functional Disulfide-Rich Peptides by Solid-Phase Synthesis and Stabilization of MRNA-Protein Fusions. *Nucleic Acids Res.* **2009**, *37* (16), e108−e108.
(78) Lamboy, J. A.; Tam, P. Y.; Lee, L. S.; Jackson, P. J.; Avrantinis, S. K.; Lee, H. J.; Corn, R. M.; Weiss, G. A. Chemical and Genetic Wrappers for Improved Phage and RNA Display. *Chembiochem* **2008**, *9* (17), 2846−2852.
(79) Guillen Schlippe, Y. V.; Hartman, M. C. T.; Josephson, K.; Szostak, J. W. In Vitro Selection of Highly Modified Cyclic Peptides That Act as Tight Binding Inhibitors. *J. Am. Chem. Soc.* **2012**, *134* (25), 10469−10477.
(80) Tanada, M.; Tamiya, M.; Matsuo, A.; Chiyoda, A.; Takano, K.; Ito, T.; Irie, M.; Kotake, T.; Takeyama, R.; Kawada, H.; Hayashi, R.; Ishikawa, S.; Nomura, K.; Furuichi, N.; Morita, Y.; Kage, M.; Hashimoto, S.; Nii, K.; Sase, H.; Ohara, K.; Ohta, A.; Kuramoto, S.; Nishimura, Y.; Iikura, H.; Shiraishi, T. Development of Orally Bioavailable Peptides Targeting an Intracellular Protein: From a Hit to a Clinical KRAS Inhibitor. *J. Am. Chem. Soc.* **2023**, *145* (30), 16610−16620.
(81) Ohta, A.; Tanada, M.; Shinohara, S.; Morita, Y.; Nakano, K.; Yamagishi, Y.; Takano, R.; Kariyuki, S.; Iida, T.; Matsuo, A.; Ozeki, K.; Emura, T.; Sakurai, Y.; Takano, K.; Higashida, A.; Kojima, M.; Muraoka, T.; Takeyama, R.; Kato, T.; Kimura, K.; Ogawa, K.; Ohara, K.; Tanaka, S.; Kikuchi, Y.; Hisada, N.; Hayashi, R.; Nishimura, Y.; Nomura, K.; Tachibana, T.; Irie, M.; Kawada, H.; Torizawa, T.; Murao, N.; Kotake, T.; Tanaka, M.; Ishikawa, S.; Miyake, T.; Tamiya, M.; Arai, M.; Chiyoda, A.; Akai, S.; Sase, H.; Kuramoto, S.; Ito, T.; Shiraishi, T.; Kojima, T.; Iikura, H. Validation of a New Methodology to Create Oral Drugs beyond the Rule of 5 for Intracellular Tough Targets. *J. Am. Chem. Soc.* **2023**, *145* (44), 24035−24051.
(82) Costales, M. G.; Haga, C. L.; Velagapudi, S. P.; Childs-Disney, J. L.; Phinney, D. G.; Disney, M. D. Small Molecule Inhibition of

https://doi.org/10.1021/jacs.5c05540
J. Am. Chem. Soc. XXXX, XXX, XXX−XXX

MicroRNA-210 Reprograms an Oncogenic Hypoxic Circuit. *J. Am. Chem. Soc.* **2017**, *139* (9), 3446−3455.

https://doi.org/10.1021/jacs.5c05540
J. Am. Chem. Soc. XXXX, XXX, XXX−XXX